Growth of Tilted Domains in an Octadecanol Langmuir Monolayer Using Radial Temperature Gradients

Z. Khattari and Th. M. Fischer*

Department of Chemistry and Biochemsitry, The Florida State University, Tallahassee, Florida 32306-4390

Received: February 6, 2004; In Final Form: April 23, 2004

Using Brewster angle microscopy, it is demonstrated that extended L_2'-single liquid crystalline domains in an octadecanol monolayer grow by locally heating and cooling Langmuir monolayers at the air/ water-interface with a focused IR-laser. The effect of the cooling rate on the domain size is discussed. The behavior is explained as an isotensile reorientation transition.

Introduction

A homogeneous body of any shape being at homogeneous temperature and free from interactions with external forces is free of stress. This fundamental statement is as simple to understand, as it is difficult to fulfill in the real world of crystal growth. In growing 3d crystals from the melt, much work has been focused on achieving a homogeneous growth of a single crystal. Usually a crystal seed is placed into a supersaturated melt and the quality of the crystal depends on the proper choice of the convective flow patterns in the vicinity of the crystal melt interface.[1] These flow patterns can be controlled by the details of the crucible and the heating and cooling mechanism used for the growth of the crystal. Usually the 3d-crystal structure itself is far from homogeneous. Sources of stress can be introduced by the agglomeration of point defects, inhomogeneous stoichiometric composition or inclusions. The largest origin of stress, however, is introduced by the requirement to extract heat out of the crystal surface. This process necessarily results in uneven temperature distributions in crystals and hence induces stresses due to inhomogeneous thermal expansions within the body.

Once a large crystal has been grown, a purification can be achieved with a zone refinement furnace. In such a furnace, one relies on a temperature gradient to drive out impurities, and also to some extent to sweep out dislocations and similar defects.

The situation is different if one considers the growth of quasi-two-dimensional crystals. Here the quasi-two-dimensional system is usually in contact with three-dimensional surroundings allowing the homogeneous heating and cooling of the two-dimensional film from the three-dimensional surroundings. Because of its negligible mass, the two-dimensional system has a negligible heat capacity such that temperature gradients are easily avoided. Examples for two-dimensional crystalline or liquid crystalline matter are found in liquid condensed and crystalline phases of Langmuir monolayers at the air/water interface.[2] Surprisingly, homogeneous heating and cooling does not necessarily result in stress free and extended 2d-liquid crystalline domains. Cyclic homogeneous annealing, however increases the size of liquid crystalline domains.[3−9] Langmuir monolayers can be described by a rich variety of competing interactions between different order parameters, such as the bond and bond orientation between the hydrophilic headgroups, the long-range orientation of the aliphatic chains, etc.[10] The competition of various interactions leads to frustration, which for the tilted phases results in a polydomain pattern of equally tilted domains of different tilt azimuth separated by domain walls where the tilt azimuth changes by approximately 60 deg.[11,12] In these systems cyclic homogeneous annealing by oscillating the surface pressure also leads to a size increase of the domains.[13]

In the present work we will show that in contrast to 3d-crystal growth, where one tries to avoid large temperature gradients, temperature gradients are essential for the growth of extended 2d-liquid crystalline domains. The monolayer is subject to a radial temperature gradient, and a tilted liquid crystalline texture is grown on the expense of an untilted liquid crystalline phase. The resulting inverted spherolitic growth can be used to produce extended single crystals.

Experimental Section

The monolayer is visualized with Brewster angle microscopy.[14,15] A second objective (20× long distance Nikon, numerical aperture = 0.2) is used for focusing a Nd:YAG infrared laser ($\lambda = 1064$ *nm*, $P \leq 1.5$ W) onto the monolayer. The focus of the IR-laser is arranged such that it coincides with the field of view of the Brewster angle microscope (BAM). The experimental apparatus has been described elsewhere.[16] The absorption of water $\alpha \approx 0.1$ cm^{-1} leads to a local heating of the monolayer. Octadecanol ($C_{18}H_{38}OH$) from Sigma-Aldrich, Deisenhofen) claimed to be 99+% pure has been used without further purification. It was spread from chloroform (p.a. Merck) onto pure water (Millipore Milli-Q at 18 MΩ) contained in the Teflon trough as described.[16]

Results and Discussion

Figure 1 shows the phase diagram of octadecanol. The phase diagrams of long chain fatty alcohols have been determined by Harkins and Copeland[17] using pressure area isotherms and later refined by Shih et al.[18] with grazing incidence X-ray diffraction (GIXD) and by Fischer, Teer, and Knobler[19] with polarized fluorescence microscopy. An isotension (constant surface tension σ) is included into the phase diagram. Generally the surface pressure

$$\pi(T,\Gamma) = \sigma_w(T) - \sigma(T,\Gamma) \quad (1)$$

depends on the temperature T and the concentration of the

* Corresponding author: tfischer@chem.fsu.edu

10.1021/jp049445q CCC: $27.50
Published on Web 06/08/2004

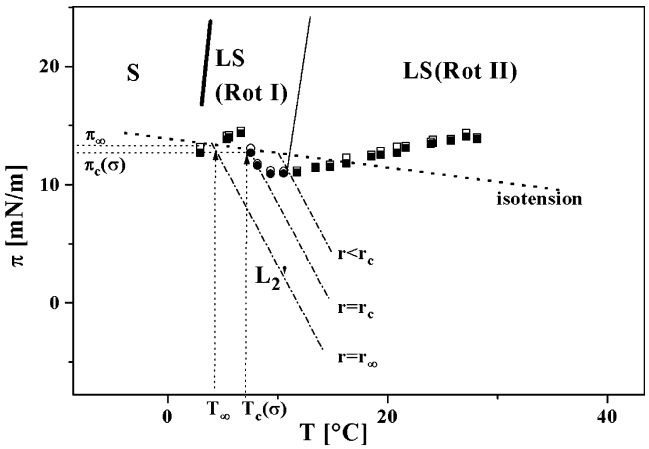

Figure 1. Phase diagram of octadecanol at the air/water interface from ref 16. The L_2'-phase is a liquid condensed phase where the tilt of the molecules is directed toward the next-nearest neighboring molecule; in all other phases the tails of the molecules are oriented perpendicular to the interface. A line of constant surface tension (isotension) is included in the phase diagram. Heating experiments presented in Figure 2 are performed along this isotension.

amphiphiles Γ, where σ and σ_w are the surface tensions of the monolayer-covered and the bare air/water interface, respectively. Hence an isotension is described by

$$\pi_{\text{isobar}}(T,\Gamma(\sigma,T)) \equiv \sigma_w(T) - \sigma \approx \pi(T_\infty,\Gamma_\infty) + \left.\frac{d\sigma_W}{dT}\right|_{T_\infty}(T - T_\infty) \quad (2)$$

where T_∞ and Γ_∞ is the reference temperature and concentration, respectively, and $d\sigma_W/dT = -0.12$ mN/mK is the slope of the bare surface tension with respect to temperature. Therefore within the phase diagram isotensions are straight lines of slope $d\sigma_w/dT$. The isotensions intersect the phase transition between the tilted and untilted phases at a temperature $T_c(\sigma)$ and surface pressure $\pi_c(\sigma)$. One may divide the isotension in a low-temperature $T < T_c(\sigma)$ and a high-temperature branch $T > T_c(\sigma)$. In most cases the low-temperature branch of the isotension is located in the untilted phase, while the high-temperature branch lies within the tilted phase. In the region of the L_2'/LS (Rot I) transition ($T_c = 6-10$ °C), this behavior is reversed. That is, isotensile heating will convert the next nearest neighbor tilted L_2'-phase into the untilted LS (Rot I) phase.

The experiments within this work have been carried out in this region at $T_\infty = 3.8$ °C and $\pi_\infty = 13.5$ mN/m, where the

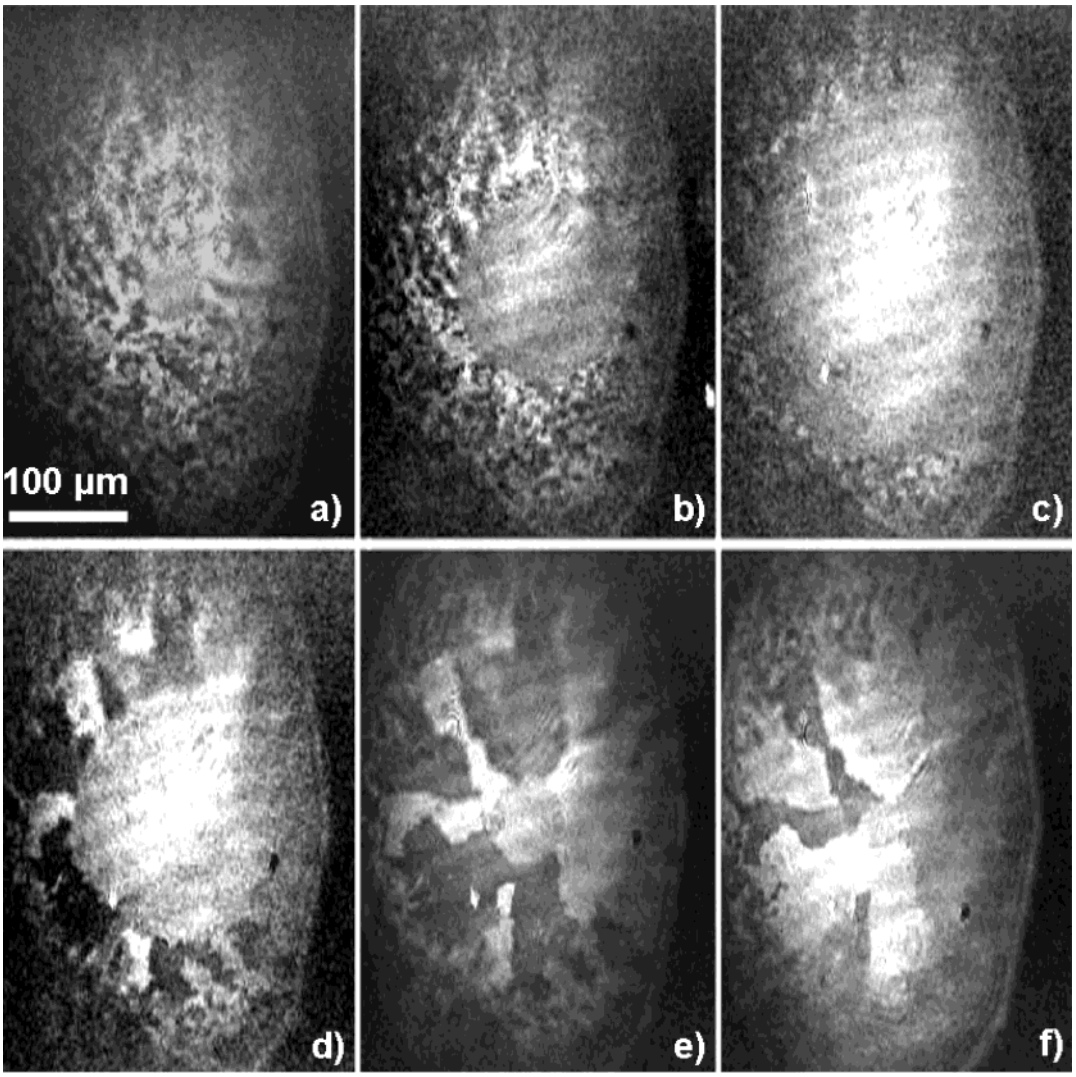

Figure 2. Brewster angle microscope images of the formation of extended 2d-liquid crystalline domains ($T_\infty = 3.8$ °C, $\pi_\infty = 13.5$ mN/m). (a) $P = 0.5$ W, a central region of untilted LS-(Rot I) phase is created appearing as average gray value in the BAM image. (b) $P = 0.6$ W The radius r_{LS} of the central region increases. (c) $P = 0.7$ W the melted LS-(Rot I) region covers almost the entire image; (d and e) cooling creates large domains of uniform tilt azimuth surrounding the central region; (f) same as panel e with rotated analyzer, demonstrating the anisotropic nature of the surrounding of the central region as well as the isotropic nature of the central phase.

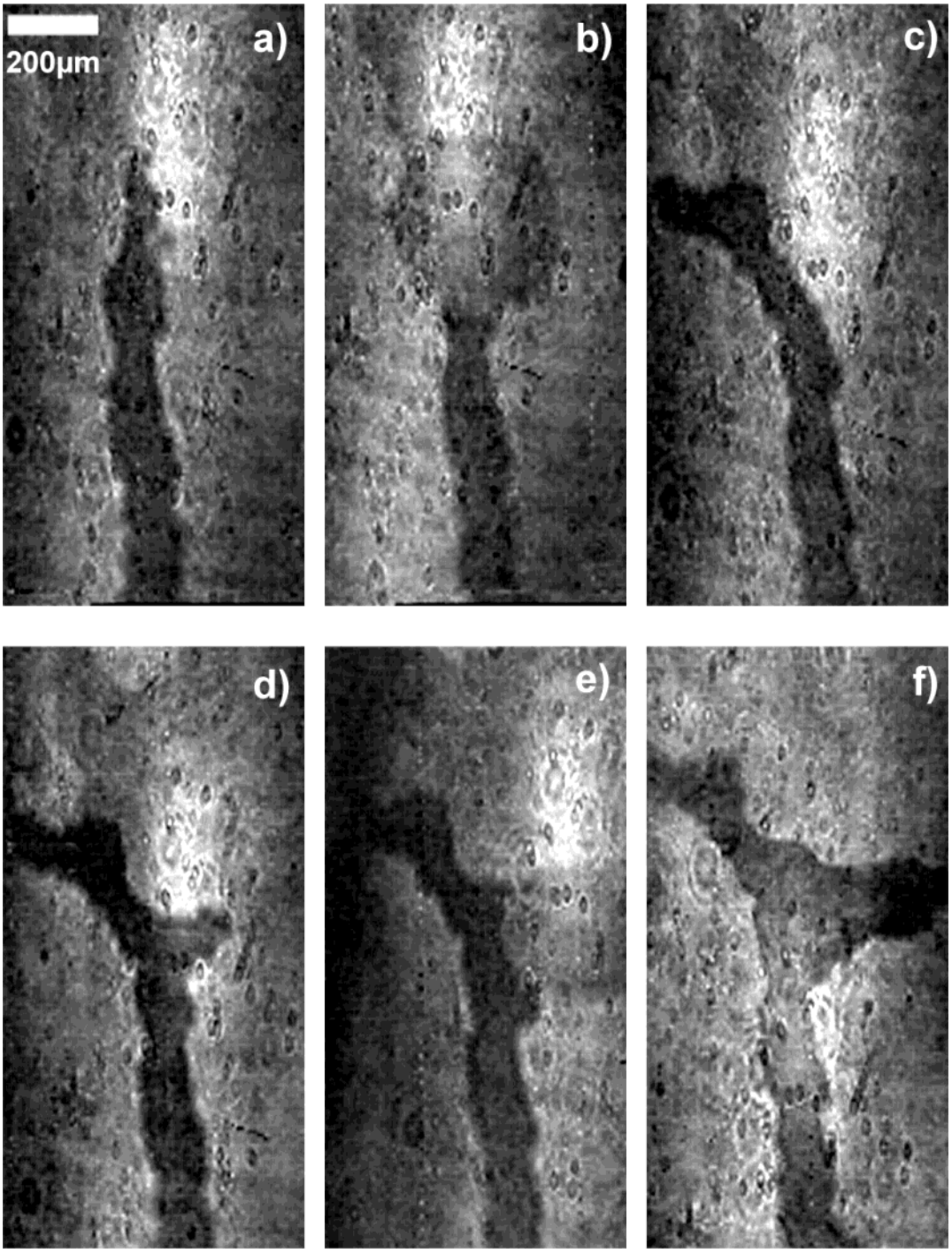

Figure 3. Writing a t-junction into the monolayer using localized laser heating. Figures a)-f) shows the consecutive stages of the patterning. In panels b and e, one can see the untilted circular region, where the laser is focused onto the monolayer.

index ∞ denotes a reference temperature and pressure measured at a radius $r_\infty \approx 50$ mm from the hot spot, i.e., the focus of the IR-laser.

Figure 2 shows the scenario of locally heating and cooling the monolayer. If the monolayer is considered as a two-dimensional liquid, then hydrostatic equilibrium requires the surface tension to be constant; i.e., any gradient in surface tension will create Marangoni forces,[20] leading to flow of the monolayer until this gradient has disappeared. Therefore the heating will be along an isotension as described by eq 2.

Figure 2a is a BAM-image of the L_2'-phase locally heated by the infrared laser ($P \approx 0.5$W). Most of the image consists of a mosaic texture of equally tilted domains of extensions of 10 μm with different tilt azimuth typical for the L_2'-phase in this region of the phase diagram. Within the center of the image a region of radius $r_c \approx 30$ μm of homogeneous gray value evolves as one turns on the heat source. While the contrast of the L_2'-mosaic pattern surrounding this region can be inverted by rotating the analyzer, the internal homogeneous region always has an intermediate gray value, which proves that the central region consists of an untilted phase. By assuming the heat to be dissipated into the subphase by heat conduction without convection, one can estimate a rise in temperature within the focus of

$$\Delta T = \alpha \frac{3P}{4\pi\kappa_W} \tag{3}$$

Here P denotes the laser power and $\kappa_W \approx 0.6$ W/mK is the

heat conductivity of water. Equation 3 predicts a rise of $\Delta T = 5.0$ K at a laser power of $P = 0.5$ W. This coincides with the amount of heating needed to reach the LS (Rot I) phase. Hence the central region consist of the untilted LS (Rot I) phase. Figure 2b,c shows the behavior on further increasing the laser power: (b) $P = 0.6$ W and (c) $P = 0.7$ W. The radius r_c increases and almost entirely covers the image at the final intensity. Heating along an isotension of somewhat higher surface tension (lower pressure) than the one depicted in Figure 1, it is also possible to get a reentrant phenomenon; i.e., the heating leads to a second crossing from the untilted LS-(Rot II) phase back to the L_2'-phase. The phase boundary there, however, is blurred since this transition is of second (weakly first[21]) order. Figure 2d−f shows the behavior when reducing the laser power, i.e., when cooling the monolayer. The radius r_c decreases and the LS-(Rot I) phase is converted back to the L_2' phase. The mosaic pattern on cooling shows L_2' domains to be larger than those of the original domains of the virgin monolayer. The radial extensions are as large as the radius r_c reached at maximum laser heating power and the pattern somewhat resembles a spherulitic crystal growth. When heating is started very close to the transition at temperatures $T_\infty = 7$ °C, then cooling creates unidirectional domains with extensions of several mm. The number of domains distributed around the central region is about 10 and depends on the speed and magnitude of the heating and cooling process. Thus the angular width of the domains is approximately 30°. An analysis of the tilt azimuth of the domains reveals that there is no preferred orientation of the domains toward the untilted phase. This suggests, that the orientation of the inverted spherulite domains is controlled by the domain walls between the L_2' domains rather than by the boundary between the L_2' domains and the central LS-(Rot I) region.

Figure 2e,f shows the morphology of the monolayer with different analyzer settings. The contrast between the L_2' domains is reversed while the central region does not change its gray value. The dependence of domain sizes on the cooling process may be demonstrated when the heating is stopped abruptly by blocking the laser beam. The resulting morphology is nondistinguishable from the virgin monolayer. Apparently low cooling rates $dT/dt < 1.0$ K/s are required to obtain large domains. Another application is to write a specific pattern into the monolayer by moving the laser focus accordingly. Figures 3a−f show the creation of a t-junction when scanning the laser spot across the monolayer. Panels a, c, d, and f are consecutive images with the laser heating switched off. Panels b and e show intermediate stages with the hotter circular untilted region, when the laser is switched on.

It is obvious that the two-dimensional crystal growth could be valuable for GIXD experiments. Our local temperature annealing technique bears advantages compared to global surface pressure annealing[13] in achieving this goal. Domains can be successively increased in size by applying the laser to the domain boundary region. If it were possible to grow a single crystal of extensions of cm, then a diffraction pattern of an oriented 2d-single crystal could be possible.

Conclusion

The combination of the focused IR-laser with BAM enables us to identify the tilt morphology in 2D. Large inverted spherulite domains of extensions up to several mm can be grown by isotensile (constant surface tension) heating and cooling with the IR-laser. The size of the domains depends on the cooling rate and the size of the untilted region.

References and Notes

(1) Hurle, D. T. J., Ed. In *Handbook of Crystal Growth, Volume 2b: Growth Mechanism and Dynamics*; North-Holland: Amsterdam, 1994.
(2) Kaganer, V. M.; Möhwald, H. *Rev. Mod. Phys*. **1999**, *71*, 779.
(3) Kajiyama, T.; Umemura, K.; Uchida, M.; Oishi, Y.; Take, R. *Chem. Lett*. **1989**, 1515.
(4) Miyano, K.; Mori, A. *Thin Solid Films* **1989**, *168*, 141.
(5) Kajiyama, T.; Oishi, Y.; Uchida, M.; Morotoni, N.; Isikawa, I.; Tanimoto, Y. *Bull. Chem. Soc. Jpn*. **1992**, *65*, 864.
(6) Shimomura, M.; Fujii, K.; Shimamura, T.; Oguchi, M.; Shinohara, E.; Nagata, Y.; Matsubara, M.; Koshiishi, K. *Thin Solid Films* **1992**, *210/211*, 98.
(7) Lu, Z. H.; Nakahara, H. *Chem. Lett*. **1995**, 117.
(8) Gutberlet, T.; Vollhardt, D. *J. Colloid Interface Sci*. **1995**, *173*, 429.
(9) Gidalewitz, D.; Mindyuk, O. Y.; Heiney, P. A.; Ocko, B. M.; Kurnaz, M. L.; Schwartz, D. K. *Langmuir* **1998**, *14*, 2910.
(10) Bibo, A. M.; Knobler, C. M.; Peterson, I. R. *J. Phys. Chem*. **1991**, *95*, 5591.
(11) Henon, S.; Meunier, J. *J. Chem. Phys*. **1993**, *98*, 9148.
(12) Fischer, Th. M.; Knobler, C. M.; Bruinsma, R. *Phys. Rev*. **1994**, *E50*, 413.
(13) Bibo, A. M.; Peterson, I. R. *Thin Solid Films* **1992**, *210*, 515.
(14) Hénon, S.; Meunier, J. *Rev. Sci. Instrum*. **1991**, *62*, 936.
(15) Hönig, D.; Möbius, D. *J. Phys. Chem*. **1991**, *95*, 4590.
(16) Lautz, C.; Kilda, J.; Fischer, Th. M. *J. Chem. Phys*. **1997**, *106*, 7448.
(17) Harkins, W. D.; Copeland, L. E. *J. Chem. Phys*. **1942**, *10*, 272.
(18) Shih, M. C.; Bohanon, T. M.; Mikrut, J. M.; Zschack, P.; Dutta, P. *J. Chem. Phys*. **1992**, *97*, 4485.
(19) Fischer, B.; Teer, E.; Knobler, C. M. *J. Chem. Phys*. **1995**, *103*, 2365.
(20) Edwards, D., Brenner, H.; Wasan, D. *Interfacial Transport Processes and Rheology*; Butterworth-Heinemann Series in Chemical Engineering; Butterworth: Boston, 1991.
(21) Lautz, C.; Fischer, Th. M.; Weygand, M.; Lösche, M.; Howes, P. B.; Kjaer, K. *J. Chem. Phys*. **1998**, *108*, 4640.